*Center for Turbulence Research*
*Proceedings of the Summer Program 1994*





# Modeling the two-point correlation of the vector stream function

By M. Oberlack[1], M. M. Rogers[2] AND W. C. Reynolds[3]

A new model for the two-point vector stream function correlation has been developed using tensor invariant arguments and evaluated by the comparison of model predictions with DNS data for incompressible homogeneous turbulent shear flow. This two-point vector stream function model correlation can then be used to calculate the two-point velocity correlation function and other quantities useful in turbulence modeling. The model assumes that the two-point vector stream function correlation can be written in terms of the separation vector and a new tensor function that depends only on the magnitude of the separation vector. The model has a single free model coefficient, which has been chosen by comparison with the DNS data. The relative error of the model predictions of the two-point vector stream function correlation is only a few percent for a broad range of the model coefficient. Predictions of the derivatives of this correlation, which are of interest in turbulence modeling, may not be this accurate.

## 1. Introduction

In one-point modeling for second-moment closure, four different terms are unknown: the pressure-strain term $\Phi_{ij}$, the dissipation term $\varepsilon_{ij}$, the pressure diffusion term ${}^{p}D_{ij}$, and the turbulent diffusion term ${}^{t}D_{ij}$. A large amount of information that is needed for closure is contained in the two-point correlation tensor $R_{ij}$. Given a model for $R_{ij}$, one can express the Reynolds stress tensor, the dissipation tensor, and the rapid part of the pressure-strain tensor as functions of $R_{ij}$:

$$\overline{u_i' u_j'} = R_{ij}(\vec{x}, \vec{r} = 0)\,, \tag{1}$$

$$\varepsilon_{ij} = \lim_{\vec{r}\to 0} \nu \left[ \frac{\partial^2 R_{ij}}{\partial x_k \partial r_k} - \frac{\partial^2 R_{ij}}{\partial r_k \partial r_k} \right]\,, \tag{2}$$

$$\Phi_{ij}^{rapid} = \frac{1}{2\pi} \int_{\mathcal{V}} \frac{\partial \bar{u}_k}{\partial x_l}(\vec{x} + \vec{r}) \left( \frac{\partial^2 R_{il}}{\partial x_j \partial r_k} - \frac{\partial^2 R_{il}}{\partial r_j \partial r_k} \right) \frac{d^3 r}{|\vec{r}|} + (i \leftrightarrow j)\,, \tag{3}$$

where $(i \leftrightarrow j)$ in Eq. (3) indicates the addition of the previous term with interchanged indices $i$ and $j$. $R_{ij}$ also provides turbulence length-scale information, including the integral length scale and the Taylor microscale.

1 Inst. für Technische Mechanik, RWTH-Aachen, Germany
2 NASA Ames Research Center
3 Center for Turbulence Research

For engineering applications it is impractical to solve the two-point correlation equation to get the required one-point information. The approach should be to extract information from the two-point correlation tensor and the two-point correlation equation in order to improve one-point models. A first step was provided by the two-point correlation equation for isotropic turbulence developed by von Kármán & Howarth (1939), which gave early insight into the decay of isotropic turbulence and the development of turbulence length scales. This isotropic tensor form was used by Crow (1969) to derive an exact expression for the rapid pressure-strain-rate correlation in isotropic turbulence. A crucial further step was taken by Naot *et al.* (1973), who extended the two-point correlation model for $R_{ij}$, which led to the linear rapid pressure-strain model utilized in the well known Launder, Reece and Rodi (1975) second-moment-closure model.

One-point turbulence models require some sort of length-scale equation. The first complete Reynolds stress model was developed by Rotta (1951a,b) in combination with a scalar integral length-scale equation. He developed the length-scale transport equation by introducing an integral operator to the trace of the two-point correlation equation. Wolfshtein (1970) has developed a similar equation. Neither Rotta or Wolfshtein introduced a model for the two-point correlation $R_{ij}$, but they did model all the sink, source, and diffusion terms on the right hand side of the length-scale equation empirically.

A completely different procedure was introduced by Donaldson and co-workers (Sandri (1977, 1978), Sandri & Cerasoli (1981), Donaldson & Sandri (1981)), who developed a new tensor length-scale equation. They approximated the correlation function $R_{ij}$ as a delta peak at zero separation and applied an integral operator to the transport equation for $R_{ij}$. This crude assumption leads to the elimination of some important terms in the tensor length-scale equation. In addition, they introduced models for some terms where exact terms can be derived.

Recently Oberlack (1994a,b) developed a new tensor length-scale equation. In his approach he has introduced a new model for the two-point correlation equation on the basis of tensor invariant theory. With this new approach the linear part of the rapid pressure-strain model could also be rederived.

The objective of this paper is twofold. First, the model introduced by Oberlack (1994a) in terms of a tensor potential will be recast in terms of the two-point correlation of the vector stream function and generalized to facilitate comparison with the DNS results. Second, the basic model assumption made by Oberlack will be evaluated by comparing the model for the two-point vector stream function correlation with DNS data of a homogeneous shear flow calculated from Rogers *et al.* (1986).

Section 2 gives an introduction to the vector stream function and discusses the non-unique behavior resulting from its definition, and then gives the definition of the basic two-point variables in correlation space and the relationship between them. Section 3 focuses on the derivation of the two-point vector stream function correlation model. A procedure to compare the model with the DNS data is outlined, and the reduction to a one parameter family of model equations is explained. Section 4

presents the results. There we introduce a new scalar measure that quantifies the difference between the DNS data and the model predictions. This quantity is used in determining the single model parameter $\gamma$.

## 2. Definition of the vector stream function

The new model for the two-point velocity correlation function introduced by Oberlack (1994a,b) had to be redefined for comparison with the DNS data of Rogers *et al.* (1986). For this purpose it is helpful to start with the vector stream function formulation.

The turbulent fluctuation velocity $u_i'$ can be expressed as the curl of the vector stream function fluctuation $\psi_i'$ (Aris 1962),

$$u_i' = \epsilon_{ijk} \frac{\partial \psi_k'}{\partial x_j} , \tag{4}$$

where $\epsilon_{ijk}$ is the alternating tensor.

Obviously any given $\psi_i'$ determines $u_i'$ uniquely, but not vice versa because any curl-free vector field $\psi_i^*$ can be added to $\psi_i'$ without changing the velocity vector $u_i'$. Thus, Eq. (4) does not define a unique $\psi_i'$, and an additional condition is required. Taking the curl of Eq. (4), we get the Poisson-like equation

$$\omega_i' = \frac{\partial^2 \psi_k'}{\partial x_i \partial x_k} - \frac{\partial^2 \psi_i'}{\partial x_k \partial x_k} , \tag{5}$$

where $\omega_i'$ is the turbulent vorticity fluctuation given by

$$\omega_i' = \epsilon_{ijk} \frac{\partial u_k'}{\partial x_j} . \tag{6}$$

Eq. (5) is fundamentally different from the standard Poisson equation, a fact that is easily seen in wavespace where the derivatives in (5) are replaced by multiplication by wavenumber components. In wavespace, the Poisson equation is a regular linear algebraic equation with a unique solution for $\psi_i'$, whereas (5) is a singular linear algebraic system that requires the specification of an additional constraint to determine $\psi_i'$. To define a well-posed problem, it is necessary to introduce an additional restriction on $\psi_i'$ as noted above.

A numerically very useful and often used condition on $\psi_i'$ is that it be solenoidal

$$\frac{\partial \psi_i'}{\partial x_i} = 0 . \tag{7}$$

By using (7), Eq. (5) reduces to the usual Poisson equation

$$\omega_i' = -\frac{\partial^2 \psi_i'}{\partial x_k \partial x_k} . \tag{8}$$

Eq. (8) has been used to determine the vector stream function from the DNS data. However, this implicit use of (7) makes it necessary to reformulate the model of the tensor potential given by Oberlack (1994a).

All the two-point correlations functions below follow the definitions of Oberlack (1994a,b). We introduce the spatial vectors $\vec{x}$ and $\vec{x}^{(1)}$ and define the correlation-space vector as

$$\vec{r} = \vec{x}^{(1)} - \vec{x} \,. \tag{9}$$

In general, the two-point correlation functions depend on the physical and the correlation space coordinates $\vec{x}$ and $\vec{r}$ and on the time $t$.

The tensor potential $V_{mn}$ introduced by Oberlack (1994a) can be expressed in terms of the two-point correlation of the vector stream function fluctuation

$$V_{mn}(\vec{x},\vec{r},t) = \overline{\psi'_m(\vec{x},t)\psi'_n(\vec{x}^{(1)},t)} \,. \tag{10}$$

$V_{mn}$ contains important length-scale information of the turbulence and can be directly linked to the two-point velocity correlation function

$$R_{ij}(\vec{x},\vec{r},t) = \overline{u'_i(\vec{x},t)u'_j(\vec{x}^{(1)},t)} \,. \tag{11}$$

$R_{ij}$ is the basic quantity in two-point modeling. The link between $V_{mn}$ and $R_{ij}$ can be found using Eq. (4) and the definition of the correlation space $\vec{r}$ given in Eq. (9),

$$R_{ij} = e_{ikm}\, e_{jln} \left[ \frac{\partial}{\partial x_k} - \frac{\partial}{\partial r_k} \right] \frac{\partial V_{mn}}{\partial r_l} \,. \tag{12}$$

The tensor potential $V_{mn}$ was originally introduced to form an $R_{ij}$ that would automatically satisfy the two equations

$$\frac{\partial R_{ij}}{\partial x_i} - \frac{\partial R_{ij}}{\partial r_i} = 0 \quad \text{and} \quad \frac{\partial R_{ij}}{\partial r_j} = 0 \tag{13}$$

emerging from the continuity condition for the turbulent velocity fluctuation $u'_i$. The constraint for the vector stream function $\psi'_i$ in Eq. (7) imposes two additional restrictions on the two-point vector stream function correlation

$$\frac{\partial V_{ij}}{\partial x_i} - \frac{\partial V_{ij}}{\partial r_i} = 0 \quad \text{and} \quad \frac{\partial V_{ij}}{\partial r_j} = 0 \,. \tag{14}$$

Oberlack (1994a,b) did not express $V_{mn}$ in terms of $\psi'_i$, and hence the constraints (14) were not implemented. It can be shown that he used an implicit constraint on the two-point vector stream function, but this is not computationally useful.

An important consequence of introducing (7) is that it becomes necessary to reformulate the model for the two-point vector stream function correlation because the model of Oberlack is not able to satisfy (14). The derivation of the generalized model is described in the next section.

## 3. Derivation of the two-point vector stream function correlation model

The ideas used here to model the two-point vector stream function correlation are similar to those introduced by Oberlack (1994a), but additional terms have been introduced to generalize the formulation. Here only homogeneous flows in infinite domains are considered, hence statistical quantities are independent of spatial location and all the spatial derivatives $\frac{\partial}{\partial x_i}$ in Eqs. (12), (13), and (14) vanish.

We seek to model the two-point vector stream function correlation $V_{mn}$ in terms of a new tensor function $G_{mn}$ and the separation vector $\vec{r}$. The components of $G_{mn}$ are all assumed to be functions only of the magnitude of the separation distance $r = |\vec{r}|$ and time $t$,

$$G_{mn} = G_{mn}(r,t)\,. \tag{15}$$

Because of the assumption (15), the tensor $G_{mn}$ has no angular variation in correlation space; the value of each component is constant on spherical shells in $\vec{r}$-space. For simplicity, $G_{mn}$ has also been assumed to be a symmetric tensor. Thus, for general homogeneous flows, $G_{mn}$ is characterized by six independent functions of $r$ and $t$. This is in contrast to isotropic turbulence, which is characterized by a single scalar function $f(r,t)$ (see Appendix).

The most general $V_{mn}$ that is linear and non-differential in the tensor $G_{mn}$ will involve the following terms:

$$G_{mn},\ \delta_{mn}G_{kk},\ \delta_{mn}\frac{r_k r_l}{r^2}G_{kl},\ \frac{r_m r_n}{r^2}G_{kk},\ \frac{r_m r_k}{r^2}G_{nk}+\frac{r_n r_k}{r^2}G_{mk},\ \frac{r_m r_n r_k r_l}{r^4}G_{kl}\,. \tag{16}$$

However, (14) can not be satisfied by an arbitrary linear combination of these forms. Therefore, we add an additional set where $G_{mn}$ is replaced by

$$G_{mn} \to r\frac{\partial G_{mn}}{\partial r}\,. \tag{17}$$

The resulting generalized form of the model is then

$$\begin{aligned}
V_{mn} - V_{mn}^{(0)} = {} & \alpha_1 G_{mn} + \beta_1 r\frac{\partial G_{mn}}{\partial r} \\
& + \alpha_2 \delta_{mn}G_{kk} + \beta_2 \delta_{mn} r\frac{\partial G_{kk}}{\partial r} \\
& + \alpha_3 \delta_{mn}\frac{r_k r_l}{r^2}G_{kl} + \beta_3\delta_{mn}\frac{r_k r_l}{r^2} r\frac{\partial G_{kl}}{\partial r} \\
& + \alpha_4 \frac{r_m r_n}{r^2}G_{kk} + \beta_4 \frac{r_m r_n}{r^2} r\frac{\partial G_{kk}}{\partial r} \\
& + \alpha_5\left[\frac{r_m r_k}{r^2}G_{nk} + \frac{r_n r_k}{r^2}G_{mk}\right] + \beta_5\left[\frac{r_m r_k}{r^2} r\frac{\partial G_{nk}}{\partial r} + \frac{r_n r_k}{r^2} r\frac{\partial G_{mk}}{\partial r}\right] \\
& + \alpha_6 \frac{r_m r_n r_k r_l}{r^4}G_{kl} + \beta_6 \frac{r_m r_n r_k r_l}{r^4} r\frac{\partial G_{kl}}{\partial r}\,.
\end{aligned} \tag{18}$$

The coefficients $\alpha_i$ and $\beta_i$ are assumed to be constants for any given field. The tensor $V_{mn}^{(0)}$ contains the value of $V_{mn}$ at $r = 0$ and has to be introduced to avoid a singularity at the origin. It does not contribute to $R_{ij}$ or other quantities of interest derived from the model because $\frac{\partial}{\partial r_i} V_{mn}^{(0)} = 0$. Throughout the rest of this paper, we have absorbed $V_{mn}^{(0)}$ into $V_{mn}$ so all elements of $V_{mn}$ drop to zero at $r = 0$ (*i.e.*, we consider the quantities $V_{mn} - V_{mn}^{(0)}$).

From its definition, $V_{mn}$ is Hermitian in homogeneous turbulence; that is $V_{mn}(\vec{r}) = V_{nm}(-\vec{r})$. The model Eq. (18) is more limited and predicts that $V_{mn}$ is symmetric since $G_{mn}$ has been assumed to be symmetric.

Because the tensors $V_{mn}$ and $G_{mn}$ are symmetric, only one condition in (14) has to be satisfied. Substituting the model (18) into (14) results in an equation containing nine independent vectors. The nine coefficients of these vectors are linear functions of $\alpha_i$ and $\beta_i$ and are set to zero to satisfy (14). This ensures that the model two-point vector stream function correlation $V_{mn}$ is consistent with the assumption of a solenoidal vector stream function.

We thus have 9 equations for the 12 coefficients $\alpha_i$ and $\beta_i$. Without any loss of generality, we have chosen $\alpha_5$, $\beta_4$, and $\beta_5$ to be the independent coefficients and have solved the equations to express the remaining nine coefficients as linear functions of these three parameters. The solution yields

$$\alpha_1 = -\frac{1}{2}\alpha_5 - \beta_5 \ , \ \alpha_2 = \frac{1}{2}\alpha_5 - 2\beta_4 - \beta_5, \ \alpha_3 = -\frac{3}{2}\alpha_5, \ \alpha_4 = -\frac{1}{2}\alpha_5,$$
$$\alpha_6 = -\frac{1}{2}\alpha_5, \ \beta_1 = -\beta_5, \ \beta_2 = -\beta_4, \ \beta_3 = -\frac{1}{4}\alpha_5 - \beta_5, \quad \text{and} \quad \beta_6 = \frac{1}{4}\alpha_5 \ . \tag{19}$$

At this point, the DNS data of Rogers *et al.* (1986) can be used to optimize the choice of the model constants $\alpha_5$, $\beta_4$, and $\beta_5$. From the DNS data, $V_{mn}$ can be calculated directly, but we also need a procedure for evaluating the six independent functions $G_{mn}$ in order to assess the quality of the model.

Eq. (18) consists of a coupled set of ordinary differential equations for $G_{mn}$. (Note that in previous formulations of the model that did not have the $r\frac{\partial G_{mn}}{\partial r}$ terms, $G_{mn}$ could be obtained by solving a system of six linear algebraic equations.) The model does not specify the functional dependence of $G_{mn}$ on $r$, and the DNS data must be used to evaluate these functions.

We have done this by equating the spherical-shell-averaged $V_{mn}$, computed from the DNS data, with the spherical-shell-averaged $V_{mn}$ predicted by the model using (18). Applying the definition of spherical-shell averaging given by

$$\overline{V}_{mn} = \frac{1}{4\pi}\int_{\Omega} V_{mn} d\Omega' = \frac{1}{4\pi}\int_0^{2\pi}\int_0^{\pi} V_{mn}\sin(\theta) d\theta d\phi \tag{20}$$

to the model expression in Eq. (18) with the constants defined in (19) yields

$$\overline{V}_{mn} = \left(\frac{1}{30}\alpha_5 - \frac{1}{3}\beta_5\right)\left(3G_{mn} + r\frac{\partial G_{mn}}{\partial r}\right) + \left(-\frac{1}{15}\alpha_5 - \frac{2}{3}\beta_4 - \frac{1}{3}\beta_5\right)\delta_{mn}\left(3G_{kk} + r\frac{\partial G_{kk}}{\partial r}\right) . \tag{21}$$

This coupled system of ordinary differential equations can be solved by splitting $G_{mn}$ into its trace $G_{kk}$ and its anisotropic part $g_{mn} = G_{mn}/G_{kk} - \delta_{mn}/3$. This decomposition decouples the differential equations for $G_{kk}$ and those for each element of $g_{mn}$. Solution of these uncoupled equations then results in the determination of $G_{mn}(r)$ in terms of the spherical-shell-averaged $\overline{V}_{mn}$

$$G_{mn} = \frac{A_1}{r^3}\int_0^r \overline{V}_{mn}r'^2 dr' + \frac{A_2}{r^3}\frac{\delta_{mn}}{3}\int_0^r \overline{V}_{kk}r'^2 dr' , \tag{22}$$

where

$$A_1 = \frac{30}{\alpha_5 - 10\beta_5} \quad \text{and} \quad A_2 = \frac{-6}{\alpha_5 + 12\beta_4 + 8\beta_5} - \frac{30}{\alpha_5 - 10\beta_5} . \tag{23}$$

All the integration constants have been set to zero to eliminate a singularity at $r = 0$.

For a given set of $\alpha_5, \beta_4$, and $\beta_5$, the functions $G_{mn}$ can be computed from the spherical-shell-averaged $\overline{V}_{mn}$ obtained from the DNS data. At this point it is clear that the functions $G_{mn}$ computed in this manner do not depend on all of $\alpha_5, \beta_4$, and $\beta_5$, but only on the reduced parameter set $(A_1, A_2)$.

To distinguish clearly between $V_{mn}$ predicted by the model (using the functions $G_{mn}$ computed from the DNS data as described above) and $V_{mn}$ calculated from the DNS data, superscripts are used. The vector stream function two-point correlation calculated from the DNS data will be labeled as $V_{mn}^{DNS}$, and that predicted by the model will be termed $V_{mn}^{model}$. Substituting $G_{mn}$ as determined from (22) into the model (18) and (19) results in the following model expression:

$$\begin{aligned} V_{mn}^{model} = \frac{3}{10\gamma - 1}\Big[&10\gamma\overline{V}_{mn} - 5(4\gamma - 1)\mathcal{R}_{mn} \\ &- (5\gamma + 1)\delta_{mn}\overline{V}_{kk} + (15\gamma - 4)\delta_{mn}\mathcal{R}_{kk} \\ &+ \frac{5}{2}(4\gamma + 1)\delta_{mn}\frac{r_k r_l}{r^2}\overline{V}_{kl} - \frac{15}{2}(4\gamma - 1)\delta_{mn}\frac{r_k r_l}{r^2}\mathcal{R}_{kl} \\ &+ (5\gamma - 1)\frac{r_m r_n}{r^2}\overline{V}_{kk} - (15\gamma - 2)\frac{r_m r_n}{r^2}\mathcal{R}_{kk} \\ &- 10\gamma\left(\frac{r_m r_k}{r^2}\overline{V}_{nk} + \frac{r_n r_k}{r^2}\overline{V}_{mk}\right) + 10(3\gamma - 1)\left(\frac{r_m r_k}{r^2}\mathcal{R}_{nk} + \frac{r_n r_k}{r^2}\mathcal{R}_{mk}\right) \\ &- \frac{5}{2}\frac{r_m r_n r_k r_l}{r^4}\overline{V}_{kl} + \frac{25}{2}\frac{r_m r_n r_k r_l}{r^4}\mathcal{R}_{kl}\Big] , \end{aligned} \tag{24}$$

where

$$\mathcal{R}_{mn} = \frac{1}{r^3}\int_0^r \overline{V}_{mn} r'^2 dr' \quad \text{and} \quad \gamma = \frac{\beta_5}{\alpha_5}\,. \tag{25}$$

Note that the model (24) does not now depend on $\alpha_4$ and that $\alpha_5$ and $\beta_5$ only appear in the ratio $\gamma$. Thus the model has only *one* free parameter that remains to be chosen by comparison with DNS data!

In the next section we compare the values of $V_{mn}$ computed directly from the DNS with those predicted by the model given by (24). This comparison is made for many values of $\gamma$ and permits the determination of an optimum value of $\gamma$ that results in the best agreement between the model predictions and the DNS data.

## 4. Results

As noted above, direct numerical simulations of incompressible homogeneous turbulent shear flow generated by Rogers *et al.* (1986) have been used both to optimize the choice of the model constant $\gamma$ and to test the validity of the model assumptions by comparing model predictions with DNS results. In these numerical simulations, the streamwise mean velocity $\overline{U}$ varies linearly in the cross-stream ($y$) direction, with the constant and uniform mean shear rate being given by $S = \partial\overline{U}/\partial y$. In this work the *C128U* simulation has been used. This case evolves until a non-dimensional time of $St = 16$, beyond which the computational domain becomes too small to capture an adequate sample of large-scale energetic turbulent eddies.

Although fields at various times $St$ have been examined, results presented here are for $St = 10$. Results at other times are qualitatively similar, but after this time the stream function (primarily from eddies of larger scale than the energy-containing eddies) begins to be limited by the computational domain size. The flow cannot be regarded as a developed shear flow before about $St = 8$.

As noted earlier, the model has been constrained to predict symmetric vector stream function two-point correlations $V_{mn}$. Therefore the DNS results have been symmetrized prior to being used for model development and evaluation (this results in only minor adjustments to the off-diagonal tensor components of $V_{mn}$).

The degree to which $V_{mn}^{DNS}$ and $V_{mn}^{model}$ are different is a measure of the quality of the model. A simple measure to quantify this difference is given by

$$p = \frac{\int_{\mathcal{V}} (V_{mn}^{model} - V_{mn}^{DNS})^2 \, d^3r}{\int_{\mathcal{V}} (V_{mn}^{DNS})^2 \, d^3r}\,, \tag{26}$$

where the integration domain $\mathcal{V}$ is restricted to a sphere of radius $r_{max}$, the largest radius that will fit into the computational domain ($r_{max} = min(L_x/2, L_y/2, L_z/2)$, where $L_i$ is the computational domain size (periodicity length) in the $i^{th}$ direction). Integration over larger separation distances is not possible because the data would be contaminated by periodic images in the computation. Note that each point in correlation space is weighted equally in the above definition. Alternative measures

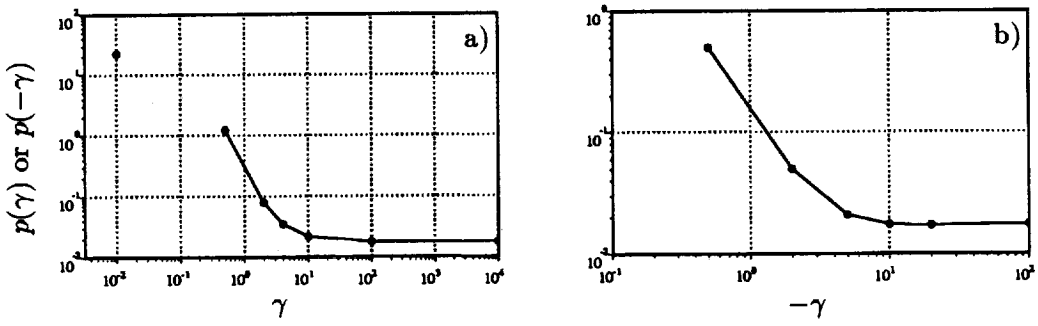


FIGURE 1. Dependence of the relative error $p$ on the parameter $\gamma$ for a) positive values of $\gamma$ and b) negative values of $\gamma$. Note that there is a singularity at $\gamma = 0.1$.

that weight the data for smaller separation distances more heavily do not change the optimum value of the model constant $\gamma$ significantly.

Fig. 1 illustrates the dependence of $p$ on the model constant $\gamma$ for both positive and negative values of $\gamma$. According to this measure, the model is equally good for both large positive and large negative values of $\gamma$, with a value of about 0.018. There is a singularity at $\gamma = 0.1$. Of the values of $\gamma$ examined (indicated by solid circles in the figure), the lowest value of $p = 0.0172$ is achieved at $\gamma = -20$. However, there is a broad minimum with many other values of $\gamma$ yielding values of $p$ that are almost this low. Other considerations discussed below suggest an optimum value of $\gamma = -5$, with $p = 0.021$. Figs. 2 and 4 have been generated using this value of $\gamma = -5$.

The qualitative form of $p(\gamma)$ for the fields at $St = 8$ and $St = 12$ is similar to that shown in Fig. 1, although the value of $p$ at the broad minimum is different. At $St = 8$, there is a minimum of $p = 0.0055$ at $\gamma = -20$; by $St = 12$, $p$ increases to 0.060 at $\gamma = -20$. By $St = 12$ the computational domain is no longer sufficiently large to capture $V_{33}$ and the increased value of $p$ is therefore not surprising.

The functions $G_{mn}$, derived as outlined in §3, are shown in Fig. 2 for the *C128U* simulation at $St = 10$ using $\gamma = -5$ ($A_1 = 20/17$, $A_2 = -800/969$). Because $V_{mn}^{(0)}$ has been subtracted from the vector stream function two-point correlation to obtain $\overline{V}_{mn}$, $\overline{V}_{mn}$ starts at zero for $r = 0$ and approaches a constant value of $-V_{mn}^{(0)}$ for large separation distances where the correlation falls to zero. Using Eq. (22), it can be shown from this that $G_{mn}$ is also zero for $r = 0$ and that the functions $G_{mn}$ will also approach constant values as the separation distance $r$ becomes large. From Fig. 2 it is clear that the tensor components $G_{12}$ and $G_{22}$ level off by $r = r_{max}$, whereas $G_{11}$ and $G_{33}$ do not. The off-diagonal components $G_{13}$ and $G_{23}$ are nearly zero compared to the other components (similar behavior is observed in the one-point correlations $\overline{u_1' u_3'}$ and $\overline{u_2' u_3'}$, which are also zero in homogeneous turbulent shear flow).

The measure $p$ indicates what good choices for the model constant $\gamma$ are, but it is also instructive to examine $V_{mn}^{model}$ directly, and to compare it with $V_{12}^{DNS}$. Fig. 3 contains contour plots of the six independent $V_{mn}^{DNS}$ components. All contour plots

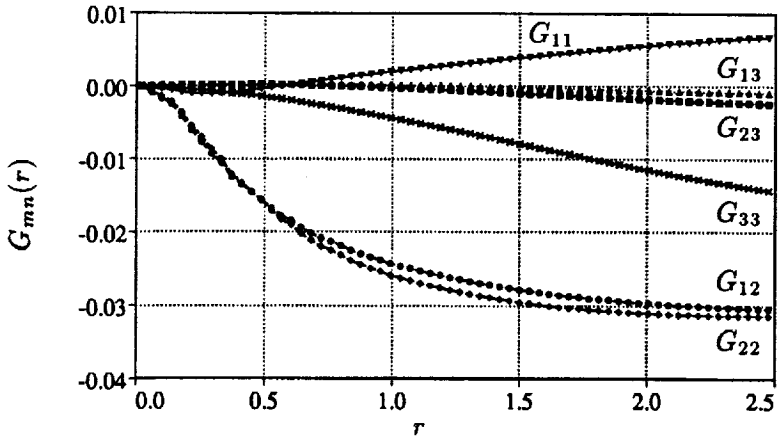


FIGURE 2. Functional dependence of $G_{mn}$ on $r$ for the *C128U* simulation at $St = 10$ and $\gamma = -5$ ($A_1 = 20/17$, $A_2 = -800/969$).

shown are in $r_x$-$r_y$-planes at $r_z = 0$. As a result of the mean shear, the contours are elongated in preferred directions. The "ridges" of the $V_{11}^{DNS}$, $V_{12}^{DNS}$, and $V_{22}^{DNS}$ contours are inclined to the streamwise direction at an angle of somewhat less than 45°, as is often the case with many quantities in this flow. The $V_{33}^{DNS}$ contours are qualitatively different, with the "ridge" running roughly orthogonal to that of the other components. Similar behavior is observed at other times $St$. The off-diagonal terms $V_{13}^{DNS}$ and $V_{23}^{DNS}$ are an order of magnitude smaller than the other terms and exhibit less organized structure; presumably they would be zero with an improved statistical sample of eddies. Examination of fields at earlier $St$ lends credence to this suggestion. At earlier times the eddies are smaller, resulting in an increased sample and improved statistics. For these fields the $V_{13}^{DNS}$ and $V_{23}^{DNS}$ components are about two orders of magnitude smaller than the others and about the same magnitude as the level of the fluctuations for large $r$ in the other components (unlike for the flow at $St = 10$, at earlier times the $V_{mn}^{DNS}$ contours are confined to a much smaller region in the center of the computational domain).

Although the measure $p$ is insensitive to the value of $\gamma$ in the range $\gamma < -10$ and $\gamma > 10$, the orientation of the contour lines for $V_{mn}^{model}$ varies significantly. The contours of $V_{mn}^{model}$ for the *C128U* simulation at $St = 10$ for $\gamma = -5$ are illustrated in Fig. 4. The model predictions are limited to the interior of a sphere of radius $r_{max}$, because the functions $G_{mn}$ cannot be determined from the DNS data for separations $r$ greater than this as noted above. For this choice of $\gamma$, the contour ridge orientations of the various components are approximately the same as those of the $V_{mn}^{DNS}$ shown in figure 3. The peak values and their decay in all directions are reasonably well represented within the radius considered. Beyond this radius, the DNS data show an increasing complexity of structures with additional secondary maxima that may be strongly influenced by the limited statistical sample of the computation and are not predicted by the model.

The orientation of the contour ridges for other values of $\gamma$ is different. When $\gamma$ is

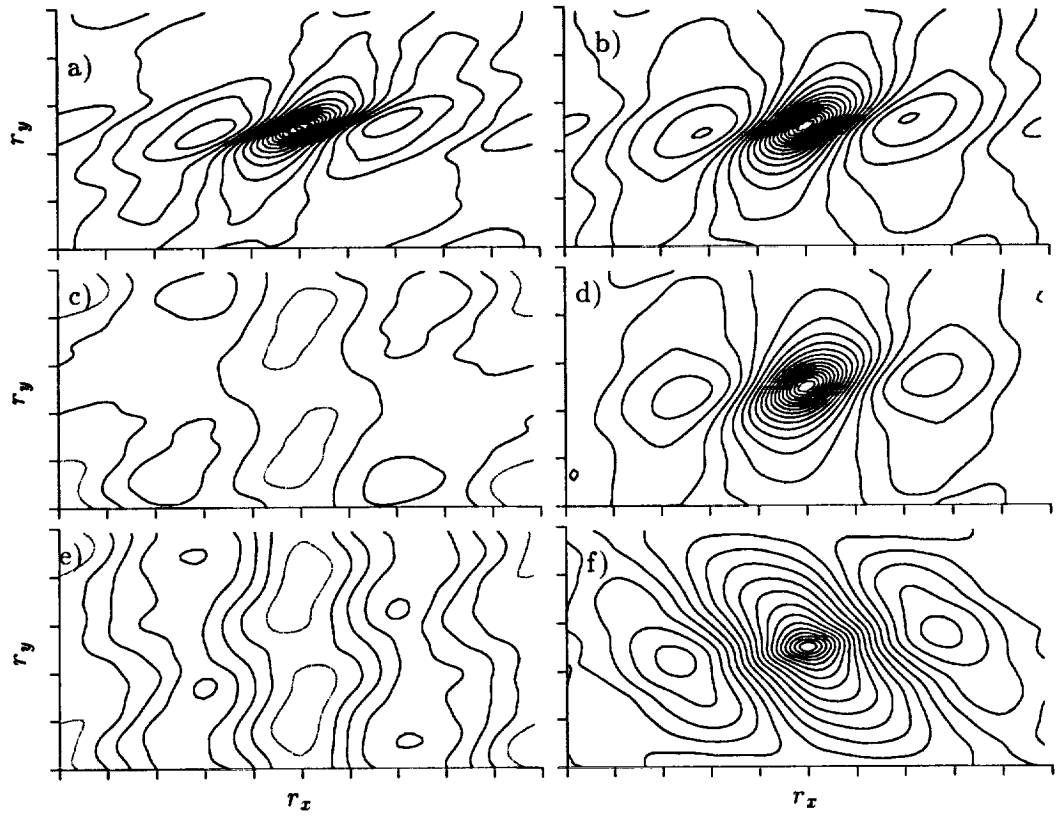


FIGURE 3. Iso-contours of a) $V_{11}^{DNS}$, b) $V_{12}^{DNS}$, c) $V_{13}^{DNS}$, d) $V_{22}^{DNS}$, e) $V_{23}^{DNS}$, and f) $V_{33}^{DNS}$ for the *C128U* simulation at $St = 10$ in the $r_x$-$r_y$-plane at $r_z = 0$. Value at the center of the domain ($r_x = 0$ and $r_y = 0$) is zero, solid contours indicate negative contour levels, and dotted contours indicate positive contour levels. Contour increments are a) 0.004, b) 0.005, d) 0.010, f) 0.010, and contours levels in c) are -0.006, -0.002, and 0.002, and in e) are -0.014, -0.010, -0.006, -0.002, and 0.002.

decreased to larger negative values, the $V_{11}^{model}$ and $V_{22}^{model}$ contours become aligned with the coordinate directions, $V_{11}^{model}$ being oriented in the streamwise direction and $V_{22}^{model}$ being oriented vertically. The $V_{12}^{model}$ and $V_{33}^{model}$ contours do not change significantly.

The $V_{mn}^{model}$ contours are the same for both large positive and large negative values of $\gamma$, but for smaller positive $\gamma$ the orientation is different from that associated with negative $\gamma$. Again, the $V_{12}^{model}$ and $V_{33}^{model}$ components are relatively unaffected by changes in $\gamma$, but for $\gamma = 2$ the contour ridges of the $V_{11}^{model}$ and $V_{22}^{model}$ components are opposite those shown in Fig. 4, *i.e.* the $V_{11}^{model}$ contours are inclined at a slightly negative angle to the streamwise direction rather than positive, and the $V_{22}^{model}$ contours are inclined to the left of the vertical axis rather than to the right. For larger positive $\gamma$ the coordinate axis-aligned contours associated with large $\gamma$ are

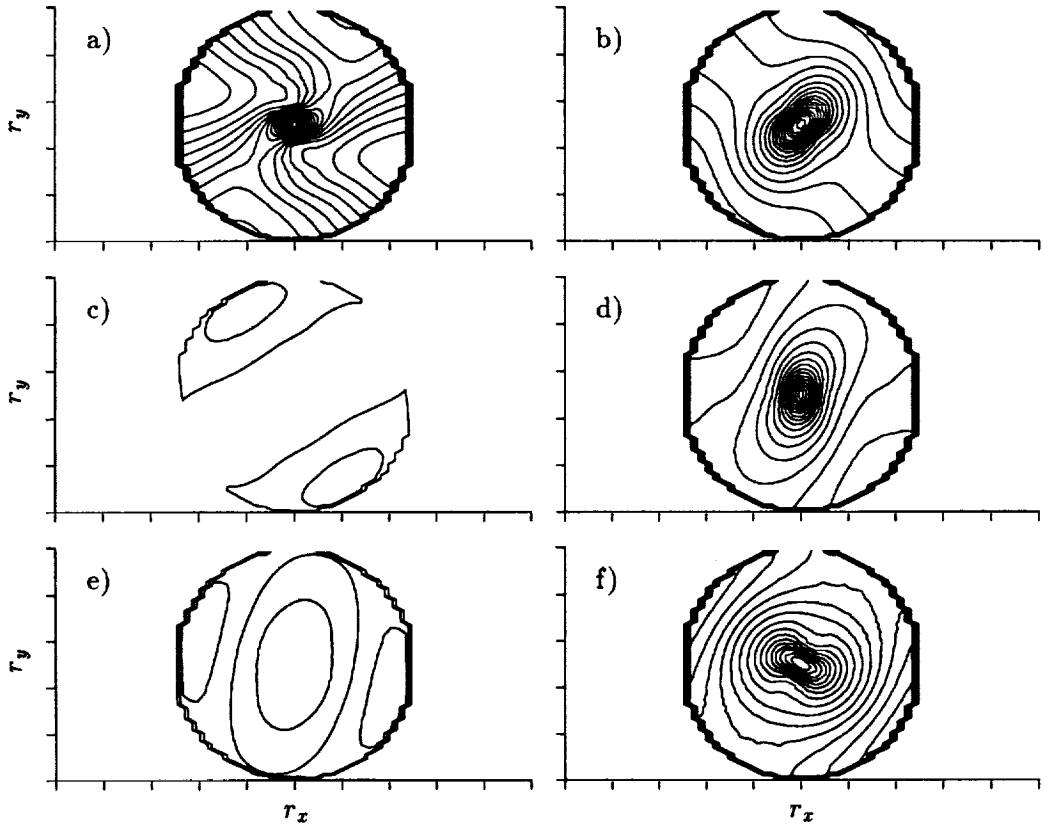


FIGURE 4. Iso-contours of a) $V_{11}^{model}$, b) $V_{12}^{model}$, c) $V_{13}^{model}$, d) $V_{22}^{model}$, e) $V_{23}^{model}$, and f) $V_{33}^{model}$ for the *C128U* simulation at $St = 10$ in the $r_x$-$r_y$-plane at $r_z = 0$ for $\gamma = -5$. Value at the center of the domain ($r_x = 0$ and $r_y = 0$) is zero, solid contours indicate negative contour levels, and dotted contours indicate positive contour levels. Contour levels are the same as in Fig. 3.

rapidly approached.

It is thus apparent that negative values of $\gamma$ should be chosen to best capture the contour orientation found in the DNS results. In this respect, this criterion leads to a similar conclusion as that based on the measure $p$ (which reaches a minimum for negative $\gamma$). However, while the measure $p$ suggests an optimum value of about $\gamma = -20$, matching the contour orientation would lead to a different choice of $\gamma$ (smaller in magnitude). From Eq. (12) it is clear that to predict accurately the two-point velocity correlation function (and thus the Reynolds stresses) we need to be able to obtain accurate estimates of *derivatives* of $V_{mn}$. Simple agreement in the magnitude of $V_{mn}$, as measured by $p$, does not ensure good prediction of the Reynolds stresses. Since virtually all quantities of interest to be computed from the model require differentiation of $V_{mn}^{model}$ to obtain, we felt that sacrificing a few tenths of a percent in $p$ in order to get the contour orientation correctly would be

justified and have taken $\gamma = -5$ as the optimum model constant as noted above. Ideally one would like to optimize the choice of $\gamma$ by comparing model predictions for the quantity of interest (*e.g.* Reynolds stress) directly with the DNS values of the same quantity. It is possible that in other flows the optimum value of $\gamma$ would be different.

## 5. Conclusions

A new model for the two-point vector stream function correlation has been developed. The proposed model has been compared with DNS data for homogeneous turbulent shear flow. The model gives a relative error $p$ of a few percent for a broad range of the single model parameter $\gamma$. A more limited range of $\gamma$ also yields the correct orientation of the two-point vector stream function correlation contours. Any integral variables (like the integral length scale) calculated from the model are relatively insensitive to the parameter $\gamma$ and should model the DNS data quite well. The model was developed for the purpose of modeling the two-point velocity correlation.

The results presented here suggest that the fundamental model assumption, namely that the two-point vector stream function correlation can be modeled in terms of the separation vector and a symmetric tensor $G_{mn}$ whose components are only a function of the magnitude of the separation vector, is justified. However, if more directional information is needed and differentiation is applied to the model predictions, the resulting quantities may have some shortcomings. An example is the rapid part of the pressure-strain correlation, which can be calculated from the model but leads to the usual linear model with its known deficiencies.

## Acknowledgements

Support was provided by the Institute für Technische Mechanik of Professor Peters at the RWTH Aachen. We would also like to thank Bob Rogallo, Claude Cambon, and Kyle Squires for helpful discussions.

## Appendix

For homogeneous isotropic turbulence the tensor $G_{mn}$ can be written in terms of a single function $G(r)$ as $G_{mn} = G(r)\delta_{mn}$. Substituting this into Eq. (18) and using (19) yields

$$V_{mn}^{model} - V_{mn}^{(0)} = \left(F(r) + \frac{r}{2}\frac{\partial F}{\partial r}\right)\delta_{mn} - \frac{r_m r_n}{r^2}\frac{r}{2}\frac{\partial F}{\partial r}\,, \qquad (A1)$$

where $F = -(\alpha_5/2+6\beta_4+4\beta_5)G$. Note that this is of the same form as the standard expression for the two-point velocity correlation tensor in isotropic turbulence

$$R_{ij} = \overline{u^2}\left[\left(f(r) + \frac{r}{2}f'(r)\right)\delta_{ij} - \frac{r}{2}f'(r)\frac{r_i r_j}{r^2}\right]\,. \qquad (A2)$$

Employing Eq. (12), we can relate the function $F(r)$ in equation (A1) to the function $f(r)$ in Eq. (A2)

$$F(r) = \frac{\overline{u^2}}{3}\left[\frac{1}{r^3}\int_0^r r'^4 f dr' - \int_0^r r' f dr'\right] . \qquad (A3)$$

## REFERENCES


ARIS, R. 1962 Vectors, tensors, and the equations of fluid mechanics. Prentice Hall, Sect. 3.43.

CROW, S. C. 1968 Viscoelastic properties of fine-grained incompressible turbulence. *J. Fluid Mech.* **33,** 1-20.

DONALDSON, C. DUP.& SANDRI, G. 1981 On the inclusion of information on eddy structure in second-order-closure models of turbulent flows. *AGARD Rep.* **CP-308,** 25.1-25.14.

VON KÁRMÁN, T. & HOWARTH, L. 1938 On the statistical theory of isotropic turbulence. *Proc. Roy. Soc.* **A 164,** 192-215.

LAUNDER, B. E., REECE, G. C. & RODI, W. 1975 Progress in the development of a Reynolds-stress turbulence closure. *J. Fluid Mech.* **68,** 537-566.

NAOT, D., SHAVIT, A. & WOLFSHTEIN, M. 1973 Two-point correlation model and the redistribution of reynolds stress. *Phys. Fluids.* **16,** 738-743.

OBERLACK, M. 1994a Closure of the dissipation tensor and the pressure-strain tensor based on the two-point correlation equation. *Turbulent Shear Flows 9,* Springer-Verlag, eds. Durst, F., Kasagi, N., Launder, B. E., Schmidt, F. W., & Whitelaw, J. H.

OBERLACK, M. 1994b Herleitung und Lösung einer Längenmaß- und Dissipations-Tensorlängenmaßgleichung für turbulente Strömungen. *Ph.D. thesis RWTH-Aachen.*

ROGERS, M. M., MOIN, P. & REYNOLDS, W. C. 1986 The structure and modeling of the hydrodynamic and passive scalar fields in homogeneous turbulent shear flow. *Thermosci. Dev., Dep. Mech. Eng.* **TF-25,** Stanford University.

ROTTA, J. C. 1951 Statistische Theorie nichthomogener Turbulenz, 1. Mitteilung. *Z. Phys.* **129,** 547-572.

ROTTA, J. C. 1951 Statistische Theorie nichthomogener Turbulenz, 2. Mitteilung. *Z. Phys.* **131,** 51-77.

SANDRI, G. 1977 A new approach to the development of scale equations for turbulent flows. *ARAP Rep.* **302.**

SANDRI, G. 1978 Recent results obtained in the modeling of turbulent flows by second-order closure. *AFOSR.* **TR-78-0680.**

SANDRI, G. & CERASOLI, C. 1981 Fundamental research in turbulent modeling. *ARAP Rep.* **438.**

WOLFSHTEIN, M. 1970 On the length-scale-of-turbulence equation. *Isr. J. Technol.* **8,** 87-99.

omit



# Rotating turbulent flows and modeling

The motivation for the group effort in this section stems from the fact that it can be shown that all one point closure models currently used in RANS (Reynolds-averaged Navier-Stokes) codes fail to correctly model the effects of strong rotation on turbulence. Yet, turbulent flows that are subjected to system rotation are found in many situations, examples are turbomachines, the wing tip vortex, geophysical flows, and many others. A prime objective of the CTR is to foster a climate where new ideas on understanding and modeling of turbulent flows will generate innovations that become part of the foundation of the turbulence knowledge base. The five papers in this section form a good example where innovations in modeling and new insights into the effects of rotation on turbulence are achieved through the use of a combination of both theory and simulations (direct and large-eddy).

Blaisdell and Shariff performed direct numerical simulations of homogeneous turbulence in elliptic streamline flow. This is a new flow in a series of building block flows where particular issues about turbulence modeling and physics are addressed. In this flow, the effects of both rotation and strain combine to provide an instability mechanism that has been proposed as a universal mechanism for energy transfer from large scales to small scales. Four cases were simulated to investigate the effects of Rossby number and ellipticity. A fifth case at high resolution was carried out to test resolution and sampling issues. Statistics of interest to turbulence modeling are presented. The simulations lead to the discovery of a homogeneous flow where the non-linear cascade is periodically suppressed and re-established.

Mahalov derived and analyzed the evolution equations for long-time averaged rotating shallow-water equations. He then used the same approach to derive equations for homogeneous flows subjected to background rotation. In this case, he decomposed the flow field into two-dimensional modes that are unaffected by rotation and three-dimensional disturbances. He showed a connection between his physical space formalism and the helical wave space formalism. The derived equations may prove useful in explaining the effects of rotation on the turbulent transfer between the scales.

Squires, Chasnov and Mansour used large-eddy simulations to investigate the asymptotic similarity of rotating homogeneous turbulence. They build on their previous investigations where, in the limit of high Reynolds number and small Rossby number, power laws for the turbulent stresses and length scales were derived based on dimensional analysis and simulation results. In the present study, a search for similarity laws for the spectra was carried out. They defined four independent energy spectra and found scalings that would collapse three out of the four spectra. The spectrum which does not collapse corresponds to two component motions in the plane normal to the rotation axis. A strong reverse cascade of the energy from small-to-large scales is found. These results hint at the tendency of the flow to become two-dimensional.

Cambon, Mansour and Squires used the same large-eddy simulations as above to investigate the development of anisotropies and the tendency of the flow to become two-dimensional. This tendency is often used as a confirmation of the Taylor-Proudman theorem. However, it can be shown that a key assumption in the derivation of the theorem does not hold for homogeneous flows. Cambon has long argued that the observed two-dimensionalization in rotating flows is a non-linear phenomenon. In the present work, results from low-Reynolds number direct numerical simulations and from high-Reynolds number large-eddy simulation are unified by arguing for the existence of two transitions in rotating turbulence that can be identified by two key Rossby numbers. During the first transition, anisotropies develop when a macro Rossby number drops below unity. During the second transition, the nonlinear transfer is shut off when a micro Rossby number drops below unity. The large-eddy simulation fields were also analyzed for alignment between vorticity fluctuations and the rotation axis. The results confirm the dominance of corrotative vorticity in the long-time high-Reynolds number limit.

Hadid, Mansour and Zeman tested a new one-point closure model that incorporates the effects of rotation on the power-law decay exponent of the turbulent kinetic energy. This modification to the $\epsilon$-equation was proposed by Zeman based on the large-eddy simulation results. During the summer program the model was successfully tested against experimental data of isotropic turbulence that was subjected to uniform rotation. A new definition of the mean rotation was proposed based on critical point theory to generalize the effects of rotation on turbulence to arbitrary mean deformations. The model was then incorporated in a code used at Rocketdyne and tested for a backward-facing step and a dump combustor. Preliminary results show promise. Further collaborations on modeling rotating flows will continue between CTR, NASA/Ames, and Rocketdyne.

N. N. Mansour